

# HUMAN-READABLE FINGERPRINT FOR LARGE LANGUAGE MODELS

Boyi Zeng<sup>1</sup>, Chenghu Zhou<sup>1</sup>, Xinbing Wang<sup>1</sup>, Zhouhan Lin<sup>1\*</sup>

<sup>1</sup>Shanghai Jiao Tong University

boyizeng@sjtu.edu.cn \*lin.zhouhan@gmail.com

## ABSTRACT

Protecting the copyright of large language models (LLMs) has become crucial due to their resource-intensive training and accompanying carefully designed licenses. However, identifying the original base model of an LLM is challenging due to potential parameter alterations. In this study, we introduce a human-readable fingerprint for LLMs that uniquely identifies the base model without exposing model parameters or interfering with training. We first observe that the vector direction of LLM parameters remains stable after the model has converged during pretraining, showing negligible perturbations through subsequent training steps, including continued pretraining, supervised fine-tuning (SFT), and RLHF, which makes it a sufficient condition to identify the base model. The necessity is validated by continuing to train an LLM with an extra term to drive away the model parameters' direction and the model becomes damaged. However, this direction is vulnerable to simple attacks like dimension permutation or matrix rotation, which significantly change it without affecting performance. To address this, leveraging the Transformer structure, we systematically analyze potential attacks and define three invariant terms that identify an LLM's base model. We make these invariant terms human-readable by mapping them to a Gaussian vector using a convolutional encoder and then converting it into a natural image with StyleGAN2. Our method generates a dog image as an identity fingerprint for an LLM, where the dog's appearance strongly indicates the LLM's base model. The fingerprint provides intuitive information for qualitative discrimination, while the invariant terms can be employed for quantitative and precise verification. Experimental results across various LLMs demonstrate the effectiveness of our method, the generated dog image remains invariant to different training steps, including SFT, RLHF, or even continued pretraining with augmented vocabulary in a new language.

## 1 INTRODUCTION

Large language models (LLMs) have become the foundation models in many scenarios of artificial intelligence. As training an LLM from scratch consumes a huge amount of computation and data resources and the trained LLM needs to be carefully protected from malicious use, the parameters of the LLMs become a crucial property to protect, for both commercial and ethical reasons. As a result, many of the LLMs are open-sourced with carefully designed licenses to reject commercial use (Touvron et al., 2023a; Taylor et al., 2022) or requiring an apply-and-approval process (Touvron et al., 2023b; Zhang et al., 2022; Penedo et al., 2023; BaiChuan-Inc, 2023; Team, 2023; Zheng et al., 2023b), let alone some LLMs are not open-sourced entirely (OpenAI, 2022; GPT-4, 2023; Brown et al., 2020; Wu et al., 2023b; Chowdhery et al., 2022; Hoffmann et al., 2022).

At the core of protecting LLMs from unauthorized use is to identify the base model of a given LLM. However, different from other forms of property such as software or images, protecting LLMs is a novel problem with unique challenges. First, the base model usually needs to be fine-tuned or even continued pretraining to be applied to downstream tasks, resulting in parameter updates that make the resulting model different from the original base model, which makes it disputable to identify the base model. Second, many of the popular LLMs are not releasing their parameters, leaving the

\*Zhouhan Lin is the corresponding author.



Figure 1: An illustrative framework for LLM protection with fingerprints. The LLM manufacturers compute the invariant terms internally, feed them to the fingerprinting model (FPM) to generate a fingerprint image, and release both to the public. This enables the public to identify shared base models both intuitively through fingerprint images and more precisely through the comparison of invariant terms. Importantly, they only disclose the invariant terms and fingerprint images, without revealing model parameters or affecting LLM training.

identification in a black-box setting. Third, different from previous smaller-scale neural networks that are only trained for specific tasks, LLMs are usually targeted for enormous forms of tasks that are not yet defined during pretraining. This has made the watermarking methods for traditional neural networks (Adi et al., 2018; Xiang et al., 2021; Yadollahi et al., 2021) not suited in this case, especially under extensive subsequent training steps.

In this work, we propose a novel way to overcome the aforementioned challenges by proposing a model that reads part of the model parameters and computes a fingerprint for each LLM, without directly exposing the LLM parameters to the public or interfering with its training process. The appearance of the fingerprint is closely dependent on the base model, and invariant to almost all subsequent training steps, including supervised fine-tuning (SFT), reinforcement learning with human feedback (RLHF), or even continue-pretraining with augmented vocabulary in a new language.

The fingerprint is based on our observation that the vector direction of LLM parameters remains stable against various subsequent training steps after the model has converged during pretraining. This makes it a good indicator for base model identification. Empirically, the sufficiency of this correlation is elaborated in Section 3.1.1, while its necessity is presented in Section 3.1.2.

Further, despite its stability towards training, the vector direction of the model parameter is vulnerable to some simple direct weight rearrangements that could significantly change the direction of parameter vectors without affecting the model’s performance. We construct three invariant terms that are robust to these weight rearrangements by systematically analyzing possible rearrangements and leveraging the Transformer structure. This is elaborated in Section 3.2.

Moreover, we make the fingerprint human-readable by mapping the invariant terms into a Gaussian random vector through a convolutional encoder and then map the Gaussian vector to a natural image through an off-the-shelf image generation model, StyleGAN2 (Karras et al., 2020). This makes our fingerprints easily interpretable and straightforward to decipher. This is elaborated in Section 4.

With this fingerprinting approach, we can sketch an outline for protecting LLMs in Figure 1.

## 2 RELATED WORKS

Despite its short history, safeguarding LLMs against unauthorized use has been a topic of significant interest. There are two primary categories of approaches.

**Post-hoc Detection** methods involve analyzing text generated by LLMs after its production. LLMdet (Wu et al., 2023a) calculates proxy perplexity by leveraging prior knowledge of the model’s next-token probabilities. DetectGPT (Mitchell et al., 2023) uses model-predicted probabilities to identify passages generated by a specific LLM. Li et al. (2023) employs perplexity scores and intricate feature engineering. These methods are usually applicable to a specific LLM and could be affected by supervised fine-tuning (SFT) and continued pretraining. More recently, Sadasivan et al. (2023) presented theoretical findings that for highly advanced AI human mimickers, even the best possible detection methods may only marginally outperform random guessing.

Model	Alpaca-Lora	Alpaca	Chinese-LLaMA	Vicuna	Baize	MedAlpaca	Koala	WizardLM	MiniGPT-4	Chinese-Alpaca	Baichuan	OpenLLaMA	InternLM	LLaMA-2
PCS	99.95	99.98	99.74	99.87	99.80	99.96	99.91	99.96	99.75	99.58	0.95	1.16	1.20	1.51
ICS	99.60	99.95	93.57	99.42	99.60	99.86	99.63	99.89	99.20	91.35	0.32	0.32	0.03	3.16

Table 1: The cosine similarities of model parameters (PCS) and Figure 2: The model’s performance quickly deteriorates as the PCS decreases.

Model	BoolQ	HellaSwag	PIQA	WinoGrande	ARC-e	ARC-c	RACE	MMLU	Avg.
LLaMA	75.11	76.19	79.16	70.00	72.90	44.80	40.00	32.75	61.36
Alpaca	77.49	75.64	77.86	67.80	70.66	46.58	43.16	41.13	62.54
+ $L_A$ (97.13)	45.44	31.16	67.63	48.70	49.03	34.13	22.78	23.13	40.25
+ $L_A$ (87.21)	42.23	26.09	49.78	47.43	26.43	28.92	22.97	23.22	33.38
+ $L_A$ (80.23)	39.05	26.40	49.95	48.30	26.52	28.75	22.97	23.98	33.24
+ $L_A$ (77.56)	41.62	26.15	50.11	49.33	26.56	28.50	22.78	23.12	33.52

Table 2: Detailed zero-shot performance on multiple standard benchmarks of the original LLaMA, Alpaca, and the tuning model at different  $L_A$ (PCS) values.

**Watermarking Techniques** can be divided into two main categories (Boenisch, 2021). The first embeds watermarks or related information into the model parameters, such as explicit watermarking scheme (Uchida et al., 2017) or leveraging another neural network (Wang et al., 2020), which could potentially affect model performance (Wang & Kerschbaum, 2019). The second category focuses on inducing unusual prediction behavior in the model. Xiang et al. (2021) explored embedding phrase triggers, and Gu et al. (2022) extended this approach to LLM; however, they are task-specific. Yadollahi et al. (2021) proposed a watermarking method but did not consider subsequent fine-tuning. Christ et al. (2023) proposed a cryptographic approach, but it is not robust to text editing. Kirchenbauer et al. (2023) involved using pre-selected tokens which inevitably alters the model prediction. These methods may turn out to be vulnerable to attacks on certain tokens, for example, Krishna et al. (2023) successfully evaded watermarking (Kirchenbauer et al., 2023), GPTZero (Tian, 2023), DetectGPT, and OpenAI’s text classifier (OpenAI, 2023) using paraphrasing attacks.

Our work doesn’t fall into any of the two categories since it is based on analyzing model weights post-hoc and relies on a wide spectrum of tokens.

### 3 VECTOR DIRECTION OF LLM PARAMETERS AND THE INVARIANT TERMS

#### 3.1 USING VECTOR DIRECTION OF LLM PARAMETERS TO IDENTIFY THE BASE MODEL

We can flatten all weight matrices and biases of an LLM into vectors, concatenate all resulting vectors together, and treat it as a single huge vector. In this subsection, we are going to show how the direction of this vector could be used to determine the base model by empirically showing its sufficiency and necessity.

##### 3.1.1 SUFFICIENCY

For sufficiency, we compute the cosine similarities between a base model LLaMA-7B and various of its offspring models, as well as other independently pretrained LLMs (Geng & Liu, 2023) that are of the same size. Table 1 shows a wide spectrum of models that inherit the LLaMA-7B base model, whose subsequent training processes involve various training paradigms, such as SFT (Taori et al., 2023; Xu et al., 2023b; Zheng et al., 2023a; Geng, 2023; Xu et al., 2023a; Han et al., 2023), SFT with LoRA (Wang, 2023) and extensive continued pretraining in a new language (Cui et al., 2023),

extending to new modalities (Zhu et al., 2023), etc. We detail the subsequent training settings of these models in Appendix Table 8.

Regardless of their various subsequent training setting, we can figure that all of these models show almost full scores in cosine similarity, largely preserving the base model’s parameter vector direction. On the other hand, the models that are trained independently appear to be completely different in parameter vector direction, showing almost zero cosine similarity with the LLaMA-7B model.

These observations indicate that a high cosine similarity between the two models highly suggests that they share the same base model, and vice versa.

### 3.1.2 NECESSITY

From the necessity perspective, we want to verify if the base model’s ability can still be preserved when the cosine similarity is intentionally suppressed in subsequent training steps. To this end, we inherit the LLaMA-7B base model and interfere with the Alpaca’s SFT process by augmenting the original SFT loss with an extra term that minimizes the absolute value of cosine similarity. i.e.

$L_A = \frac{|\langle \mathbf{V}_A, \mathbf{V}_{base} \rangle|}{\|\mathbf{V}_A\| \|\mathbf{V}_{base}\|}$ . Here  $\mathbf{V}_A, \mathbf{V}_{base}$  stand for the parameter vector of the model being tuned and that of the base model, respectively.

Figure 2 presents the average zero-shot performance on a set of standard benchmarks when  $L_A$ (PCS) is at different values. The benchmarks include BoolQ (Clark et al., 2019), PIQA (Bisk et al., 2020), HellaSwag (Zellers et al., 2019), WinoGrande (Sakaguchi et al., 2021), ARC-e, ARC-c (Clark et al., 2018), RACE (Lai et al., 2017) and MMLU (Hendrycks et al., 2020). Table 2 details the performance on each task during SFT. We can see that despite the original training loss is still present, the model quickly deteriorates to random guesses as the cosine similarity detaches away from that of the base model.

These observations indicate that it is fairly hard for the model to preserve the base model’s performance without keeping a high cosine similarity to it.

## 3.2 DERIVING THE INVARIANT TERMS

Although the vector direction of model parameters is shown to closely stick to its base model, directly comparing the vector direction through cosine similarity requires both models to reveal their parameters, which is unacceptable in many cases. In addition, apart from training, parameter vector direction is vulnerable to some attacks that directly rearrange the model weights. For example, since the hidden units in a model layer are permutation-invariant, one can easily alter the parameter vector direction by randomly permuting the hidden units along with the weights wired to the units. These attacks are invisible to discover since they could easily break the cosine similarity but neither change the model structure nor affect the model performance.

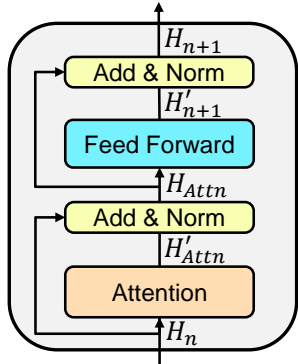


Figure 3: Transformer layer

is the self-attention output. To reduce clutter, we omit equations related to residual connection and LayerNorm, but denote the variables right before it with an apostrophe. The  $\mathbf{W}$ ’s and  $\mathbf{b}$ ’s are weights and biases.

In this subsection, we are going to first systematically analyze and formalize possible weight rearrangements by leveraging the structure constraints of the Transformer, and then derive three terms that are invariant under these rearrangements, even when they are combined. Let’s first consider the Transformer layer as depicted in Figure 3. Formally, the layer conducts the following computation:

$$\mathbf{H}'_{Attn} = \text{softmax} \left( \frac{\mathbf{H}_n \mathbf{W}_Q (\mathbf{H}_n \mathbf{W}_K)^T}{\sqrt{d}} \right) \mathbf{H}_n \mathbf{W}_V \mathbf{W}_O \quad (1)$$

$$\mathbf{H}'_{n+1} = \sigma (\mathbf{H}'_{Attn} \mathbf{W}_1 + \mathbf{b}_1) \mathbf{W}_2 + \mathbf{b}_2 \quad (2)$$

where  $\mathbf{H}_n \in \mathbb{R}^{l \times d}$  is the hidden state of the  $n$ -th layer, with  $l, d$  being sequence length and model dimensions, respectively.  $\mathbf{H}'_{Attn}$

Note that the first layer reads the word embedding, i.e.,  $\mathbf{H}_0 = \mathbf{X} \in \mathbb{R}^{l \times d}$ , and the final output distribution  $\mathbf{P} \in \mathbb{R}^{l \times v}$  is given by

$$\mathbf{P} = \text{softmax}(\mathbf{H}_N \mathbf{E}) \quad (3)$$

where  $v$  is the vocabulary size,  $N$  is the total number of layers, and  $\mathbf{E} \in \mathbb{R}^{d \times v}$  is the parameter matrix in the softmax layer, which is sometimes tied with the word embedding matrix at the input.

### 3.2.1 FORMS OF WEIGHT REARRANGEMENT ATTACKS

Putting Equation 1 ~ Equation 3 together, we can systematically analyze how the parameter vector direction can be attacked through direct weight rearrangements. There are totally 3 forms of attacks that could camouflage the model without changing its architecture or affecting its output.

**1. Linear mapping attack on  $\mathbf{W}_Q$ ,  $\mathbf{W}_K$  and  $\mathbf{W}_V$ ,  $\mathbf{W}_O$ .** Consider Equation 1, one can transform  $\mathbf{W}_Q$  and  $\mathbf{W}_K$  symmetrically so that the product  $\mathbf{W}_Q \mathbf{W}_K^T$  remains unchanged but both weights are significantly modified. This will alter the parameter vector direction significantly. Formally, for any invertible matrix  $\mathbf{C}_1$ , let

$$\tilde{\mathbf{W}}_Q = \mathbf{W}_Q \mathbf{C}_1, \quad \tilde{\mathbf{W}}_K = \mathbf{W}_K \mathbf{C}_1^{-1} \quad (4)$$

and substitute them respectively into the model, one can camouflage it as if it's a brand new model, without sacrificing any of the base model's performance. The same holds for  $\mathbf{W}_V$ ,  $\mathbf{W}_O$  as well.

**2. Permutation attack on  $\mathbf{W}_1$ ,  $\mathbf{b}_1$ ,  $\mathbf{W}_2$ .** Consider Equation 2, since it consists of two fully connected layers, one can randomly permute the hidden states in the middle layer without changing its output. Formally, let  $\mathbf{P}_{FFN}$  be an arbitrary permutation matrix, one can camouflage the model without sacrificing its performance by substituting the following three matrices accordingly

$$\tilde{\mathbf{W}}_1 = \mathbf{W}_1 \mathbf{P}_{FFN}, \quad \tilde{\mathbf{W}}_2 = \mathbf{P}_{FFN}^{-1} \mathbf{W}_2, \quad \tilde{\mathbf{b}}_1 = \mathbf{b}_1 \mathbf{P}_{FFN} \quad (5)$$

**3. Permutation attack on word embeddings.** In a similar spirit, one can permute the dimensions in the word embedding matrix as well, although it would require all remaining parameters to be permuted accordingly. Formally, let  $\mathbf{P}_E$  be an arbitrary permutation matrix that permutes the dimensions in  $\mathbf{X}$  through  $\tilde{\mathbf{X}} = \mathbf{X} \mathbf{P}_E$ , due to the existence of the residual connections, the output of all layers have to be permuted in the same way, i.e.,  $\tilde{\mathbf{H}}_n = \mathbf{H}_n \mathbf{P}_E$ . Note that it's not necessarily the case in the former two types of attacks. This permutation has to be canceled out at the final softmax layer (Equation 3), by permuting the dimensions in  $\mathbf{E}$  accordingly, i.e.  $\tilde{\mathbf{E}} = \mathbf{P}_E^{-1} \mathbf{E}$ . Specifically, all remaining parameters have to be permuted in the following way:

$$\begin{aligned} \tilde{\mathbf{W}}_Q &= \mathbf{P}_E^{-1} \mathbf{W}_Q, & \tilde{\mathbf{W}}_K &= \mathbf{P}_E^{-1} \mathbf{W}_K, & \tilde{\mathbf{W}}_V &= \mathbf{P}_E^{-1} \mathbf{W}_V, & \tilde{\mathbf{W}}_O &= \mathbf{W}_O \mathbf{P}_E \\ \tilde{\mathbf{W}}_1 &= \mathbf{P}_E^{-1} \mathbf{W}_1, & \tilde{\mathbf{W}}_2 &= \mathbf{W}_2 \mathbf{P}_E, & \tilde{\mathbf{b}}_2 &= \mathbf{b}_2 \mathbf{P}_E \end{aligned} \quad (6)$$

Moreover, putting everything together, one can combine all the aforementioned three types of attacks altogether. Formally, the parameters can be camouflaged as:

$$\begin{aligned} \tilde{\mathbf{W}}_Q &= \mathbf{P}_E^{-1} \mathbf{W}_Q \mathbf{C}_1, & \tilde{\mathbf{W}}_K &= \mathbf{P}_E^{-1} \mathbf{W}_K \mathbf{C}_1^{-T}, & \tilde{\mathbf{W}}_V &= \mathbf{P}_E^{-1} \mathbf{W}_V \mathbf{C}_2, & \tilde{\mathbf{W}}_O &= \mathbf{C}_2^{-1} \mathbf{W}_O \mathbf{P}_E \\ \tilde{\mathbf{W}}_1 &= \mathbf{P}_E^{-1} \mathbf{W}_1 \mathbf{P}_{FFN}, & \tilde{\mathbf{b}}_1 &= \mathbf{b}_1 \mathbf{P}_{FFN}, & \tilde{\mathbf{W}}_2 &= \mathbf{P}_{FFN}^{-1} \mathbf{W}_2 \mathbf{P}_E, & \tilde{\mathbf{b}}_2 &= \mathbf{b}_2 \mathbf{P}_E \\ \tilde{\mathbf{X}} &= \mathbf{X} \mathbf{P}_E, & \tilde{\mathbf{E}} &= \mathbf{P}_E^{-1} \mathbf{E} \end{aligned} \quad (7)$$

Note that for permutation matrix we have  $\mathbf{P}^{-1} = \mathbf{P}^T$ . This includes all possible attacks that 1) do not change the model architecture, and 2) do not affect the model's output.

### 3.2.2 THE INVARIANT TERMS TO THESE ATTACKS

To find the invariant terms under all these attacks, we need to combine terms in Equation 7 to get the invariant term that nicely cancels out all extra camouflaging matrices. To this end, we construct 3 invariant terms:

$$\mathbf{M}_a = \hat{\mathbf{X}} \mathbf{W}_Q \mathbf{W}_K^T \hat{\mathbf{X}}^T, \quad \mathbf{M}_b = \hat{\mathbf{X}} \mathbf{W}_V \mathbf{W}_O \hat{\mathbf{X}}^T, \quad \mathbf{M}_f = \hat{\mathbf{X}} \mathbf{W}_1 \mathbf{W}_2 \hat{\mathbf{X}}^T \quad (8)$$

Note that for  $\hat{\mathbf{X}}$  in these terms, we don't include all tokens from a vocabulary or tokens in a specific sentence; instead, we select a subset of tokens. There are two problems if we directly use all tokens'

embeddings  $\mathbf{X}$ . First, using the whole embedding matrix will make the terms unnecessarily large and of variable size between different models. Second, more importantly, since it is common to inherit a base model with an augmented vocabulary, i.e., to append a set of new tokens at the end of the original vocabulary, the invariant terms would have different sizes and be incomparable. Third, if we designate specific tokens instead, the selected tokens may not always exist in all LLMs being tested. Consequently, we carefully choose the tokens to be included in  $\hat{\mathbf{X}}$ , by following these steps:

1. Select a sufficiently big corpus as a standard verifying corpus.
2. Tokenize the corpus with the LLM’s vocabulary and sort all tokens in the vocabulary according to their frequency.
3. Delete all tokens in the vocabulary that don’t show up in the corpus.
4. Among the remaining tokens, select the least frequent  $K$  tokens as the tokens to be included in  $\hat{\mathbf{X}}$ .

Here, using a standard corpus ensures that the resulting tokenization will be identical if a certain model’s vocabulary is a subset of another; the sufficiently large corpus stabilizes the frequencies of tokens in the vocabulary and provides enough chance for as many tokens as possible to show up. Deleting zero-shot tokens automatically sweeps off augmented tokens. Selecting the rarest tokens minimizes potential affections brought by parameter updates in subsequent training processes. A properly large  $K$  will ensure a large enough set of tokens is included, making the resulting invariant terms more generally representative. More importantly, it will make all the invariant terms have the same size across all LLMs, regardless of their original sizes. In practice, we choose  $K = 4096$ .

We show the cosine similarity between the invariant terms in [Table 1](#). Although not as perfect as the parameter’s cosine distances, they still preserve a high correlation to the base model.

## 4 MAKING THE INVARIANT TERMS HUMAN-READABLE: THE FINGERPRINTING MODEL

Instead of directly using the three invariant terms, we can present the content in the terms in a human-readable way, through the fingerprinting model. The fingerprinting model consists of a neural network encoder - a convolutional encoder in our case - and an off-the-shelf image generator as depicted in [Figure 4](#). In principle, the encoder takes as input the invariant terms of a certain model, tile them together, and deterministically maps them to a vector that appears to be filled with Gaussian variables. The subsequent image generator reads this vector and maps it to a natural image. Importantly, throughout the process, the locality of the inputs has to be preserved from end to end. i.e., similar invariable terms should result in similar Gaussian variables and finally similar images.

### 4.1 TRAINING THE CONVOLUTIONAL ENCODER

All the invariant terms in [Equation 8](#) have the same size, i.e.,  $M_a, M_b, M_f \in \mathbb{R}^{K \times K}$ , regardless of the index of the layer or LLM sizes. As a result, we can tile up them to form a 3D input tensor  $M \in \mathbb{R}^{K \times K \times C}$ , where  $C$  is the channel dimension. If we are using all layers,  $C = 3N$ . Again, in order to make  $M$  the same size across all models, we only involve the last  $r$  layers in the LLM<sup>1</sup>.

Note that we don’t need to use any real LLM weights for training the convolutional encoder, as it only needs to learn a locality-preserving mapping between the input tensor and the output Gaussian vector. This ensures strict exclusivity between the training and test data. To construct the training data, we synthesize the matrix in each channel of  $M$  on-the-fly, by randomly sampling 3 matrices  $P_1, P_2, P_3$  and multiplying them together as  $P_1 P_2 P_3 P_1^T$ , as though they are model parameters.

To learn locality-preserving mapping, we adopt contrastive learning. For a randomly sampled input  $M$ , its negative sample is given by another independently sampled tensor  $M^-$ . For its positive sample  $M^+$ , we perturb the content in each of  $M$ ’s channel by adding small perturbation noises  $\epsilon_i \in \mathcal{N}(0, \alpha)$  to the 3 matrices behind it. Following is the detailed process.

<sup>1</sup>In fact, experimentally we find that a small  $r$  is already sufficient to discriminate LLMs, it’s not necessary to involve many layers. In all of our experiments,  $r = 2$ , so there are only 6 channels in the input.

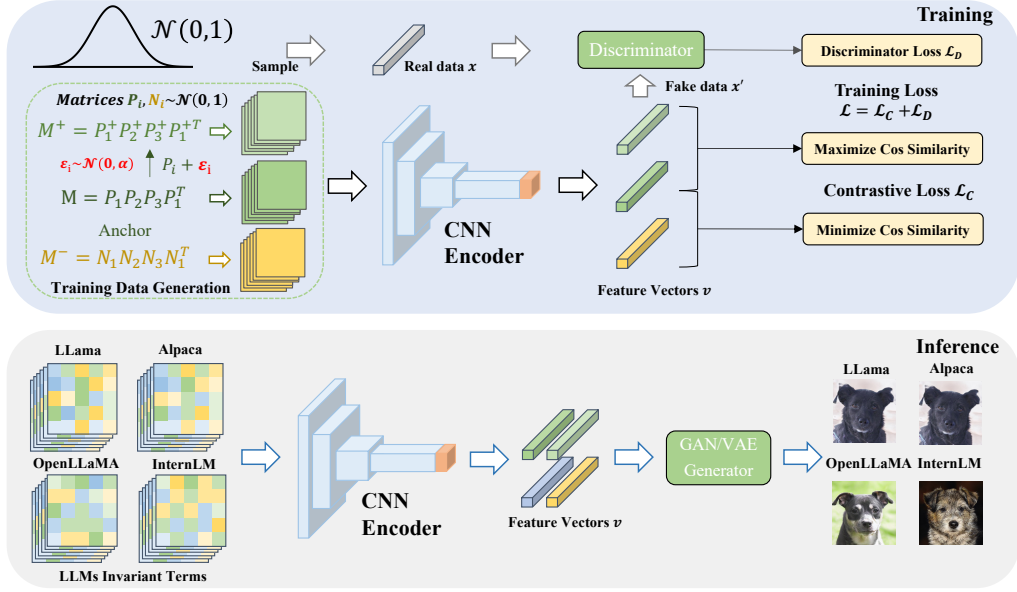


Figure 4: The training and inference of our fingerprinting model.

For the anchor data  $M$ : Sample matrices  $P_1, P_2, P_3$  from a standard normal distribution. Consider  $P_1$  as  $\hat{X}$ , and  $P_2, P_3$  as model parameter matrices, then

$$M = P_1 P_2 P_3 P_1^T \quad (9)$$

For positive data  $M^+$ : Independently sample noises  $\epsilon_i$  from a normal distribution  $\mathcal{N}(0, \alpha)$ , then

$$P_i^+ = P_i + \epsilon_i, \quad M^+ = P_1^+ P_2^+ P_3^+ P_1^{+T} \quad (10)$$

For negative data  $M^-$ : Independently sample matrices  $N_1, N_2, N_3$  from another standard normal distribution, then

$$M^- = N_1 N_2 N_3 N_1^T \quad (11)$$

Here  $\alpha$  is a hyperparameter determining the small variance. Subsequently, the contrastive loss  $\mathcal{L}_C$  is given by:

$$\mathcal{L}_C = |(1 - S_C(M, M^+))| + |S_C(M, M^-)| \quad (12)$$

where  $S_C(\cdot, \cdot)$  computes the cosine similarity between its two input matrices.

To render the output vector to be Gaussian, we adopt the standard GAN (Karras et al., 2019) training scheme. We add a simple MLP as the discriminator  $D$  that is trained to discriminate between real Gaussian vectors and the convolutional output vector  $v$ . In this setting, the convolutional encoder serves as the generator. During training, for every  $m$  step, we alternate between training the discriminator and the generator. The discriminator loss  $\mathcal{L}_D$  is thus given by

$$\mathcal{L}_D = \frac{1}{m} \sum_{i=1}^m \log(1 - D(v)) \quad (13)$$

While training the generator we also need to incorporate the contrastive learning loss. Thus the actual loss  $\mathcal{L}$  for the training generator is a combination of  $\mathcal{L}_C$  and  $\mathcal{L}_D$ .

$$\mathcal{L} = \mathcal{L}_C + \mathcal{L}_D \quad (14)$$

## 4.2 INFERENCE

In the inference stage, the convolutional encoder takes the invariant terms from real LLMs and outputs  $v$ . One image generator converts  $v$  into a natural image. In principle, any image generator

Base Model	Falcon-40B	LLaMA2-13B	MPT-30B	LLaMA2-7B	Qwen-7B	Baichuan-13B	InternLM-7B
Offspring1	99.61	99.50	99.99	99.47	98.98	99.76	99.28
Offspring2	99.69	99.49	99.99	99.41	99.71	99.98	99.02

Table 3: The cosine similarities of invariant terms (ICS) between offspring models and their corresponding base model.

that takes a Gaussian input and has the locality-preserving property would fit here. By visually representing the invariant terms as fingerprints, we can easily identify base models based on their fingerprint images, enabling reliable tracking of model origins. In this paper, we employ the StyleGAN2 generator pretrained on the AFHQ (Choi et al., 2020) dog dataset to generate natural images, following is a detailed description of it.

StyleGAN2 is an improved model based on the style-based GAN architecture. One of its key enhancements is the incorporation of the perceptual path length (PPL) metric, which was originally introduced to quantify the smoothness of the mapping from the latent space to the output image. The PPL metric measures the average LPIPS distances (Zhang et al., 2018) between generated images under small perturbations in the latent space. Through the utilization of path length regularization, StyleGAN2 achieves enhanced reliability, consistency, and robustness, resulting in a smoother behavior of the generator. This regularization technique aligns with our objective of obtaining a locality-preserving generator.

## 5 EXPERIMENTS

Our experiments are threefold. First, we validate the effectiveness of invariant terms as quantitative fingerprints. Second, we generate human-readable fingerprints for LLMs and evaluate their ability for qualitative discrimination. Finally, we validate the uniqueness and stability of the parameter direction of independently trained LLMs on a smaller scale.

### 5.1 INVARIANT TERMS AS QUANTITATIVE FINGERPRINT

In this section, we validate the effectiveness and robustness of invariant terms as quantitative fingerprints through four key experiments. First, we compute the Invariant Terms’ Cosine Similarity (ICS) between several widely used open-sourced LLM base models and their offspring LLMs. Second, we assess our method on the LLaMA model family, including heavily continue-pretrained models, to experimentally verify its robustness against subsequent training processes. Third, we conduct extensive experiments on additional open-sourced LLMs, showcasing low ICS between independently trained models. Finally, we gather 51 offspring models and calculate the accuracy of correctly identifying the base model. For all invariant terms, we use the last two layers’ parameters and set  $K = 4096$ , resulting in  $\mathbf{M} \in \mathbb{R}^{4096 \times 4096 \times 6}$  for all models.

#### 5.1.1 INDEPENDENTLY TRAINED LLMs AND THEIR OFFSPRING MODELS

We perform experiments on 7 commonly used open-sourced LLMs, ranging in size from 7B to 40B. The 7 base models considered are Falcon-40B (Almazrouei et al., 2023), MPT-30B (Lin et al., 2022), LLaMA2-7B, 13B, Qwen-7B (Bai et al., 2023), Internlm-7B and Baichuan-13B. For each of these base models, we collect 2 popular offspring models.

We extract the invariant terms for all these models and calculate the ICS for each offspring model w.r.t. its base model (Table 3). Remarkably, all offspring models exhibit very high ICS, indicating significant similarity in their invariant terms w.r.t. their respective base models.

#### 5.1.2 LLAMA AND ITS OFFSPRING MODELS

To assess the robustness of our proposed method under diverse subsequent training processes, we leverage the LLaMA-7B base model as a testing ground due to its widespread use and extensive family of offspring models. We include ten offspring models detailed in Section 3.1.1 and add Beaver, Guanaco (Dettmers et al., 2023), and BiLLa (Li, 2023) to the collection. See Appendix Table 8



ICS	LLaMA	MiGPT	Alpaca	MAlpaca	Vicuna	Wizard	Baize	AlpacaL	CAlpaca	Koala	CLLaMA	Beaver	Guanaco	BiLLa
LLaMA	100.00	99.20	99.95	99.86	99.42	99.89	99.60	99.60	91.35	99.63	93.57	99.97	92.62	82.56
MiGPT	99.20	100.00	99.17	99.10	99.10	99.15	98.83	98.82	90.65	99.00	92.84	99.19	91.93	82.24
Alpaca	99.95	99.17	100.00	99.82	99.38	99.85	99.55	99.57	91.31	99.59	93.53	99.97	92.59	82.52
MAlpaca	99.86	99.10	99.82	100.00	99.31	99.76	99.46	99.47	91.23	99.51	93.45	99.84	92.50	82.51
Vicuna	99.42	99.10	99.38	99.31	100.00	99.35	99.05	99.04	90.84	99.15	93.04	99.41	92.14	82.28
Wizard	99.89	99.15	99.85	99.76	99.35	100.00	99.50	99.50	91.25	99.56	93.47	99.87	92.52	82.57
Baize	99.60	98.83	99.55	99.46	99.05	99.50	100.00	99.23	90.97	99.25	93.19	99.57	92.25	82.25
AlpacaL	99.60	98.82	99.57	99.47	99.04	99.50	99.23	100.00	90.99	99.24	93.21	99.59	92.31	82.30
CAlpaca	91.35	90.65	91.31	91.23	90.84	91.25	90.97	90.99	100.00	91.04	97.44	91.33	85.19	75.60
Koala	99.63	99.00	99.59	99.51	99.15	99.56	99.25	99.24	91.04	100.00	93.23	99.61	92.27	82.34
CLLaMA	93.57	92.84	93.53	93.45	93.04	93.47	93.19	93.21	97.44	93.23	100.00	93.55	86.80	77.41
Beaver	99.97	99.19	99.97	99.84	99.41	99.87	99.57	99.59	91.33	99.61	93.55	100.00	92.60	82.57
Guanaco	92.62	91.93	92.59	92.50	92.14	92.52	92.25	92.31	85.19	92.27	86.80	92.60	100.00	77.17
BiLLa	82.56	82.24	82.52	82.51	82.28	82.57	82.25	82.30	75.60	82.34	77.41	82.57	77.17	100.00

Table 4: The cosine similarities of invariant terms (ICS) between various pairs of LLaMA-7B and its offspring models. Abbreviations: MedAlpaca (MAlpaca), Alpaca-Lora (AlpacaL), MiniGPT-4 (MiGPT), WizardLM (Wizard), Chinese-Alpaca (CAlpaca), Chinese-LLaMA (CLLaMA).

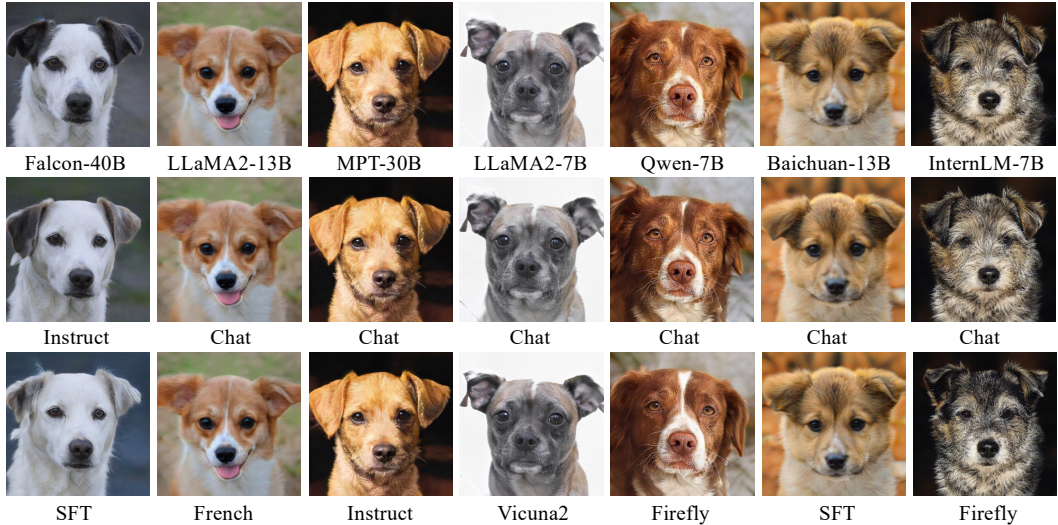


Figure 5: Fingerprints of 7 different base models (in the first row) and their corresponding offspring models (the lower two rows) are presented. The base model’s name is omitted in the offspring models.

for detailed descriptions. We extract invariant terms following the previous settings and compute the cosine similarity of the invariant terms (ICS) between each pair of models. Despite undergoing various training paradigms, such as RLHF, SFT, modality extension, and continued pretraining in a new language, we observe a high degree of similarity, with an **average ICS** of **94.14** (excluding diagonal elements).

### 5.1.3 A WIDER COLLECTION OF INDEPENDENTLY TRAINED LLMs

Besides the aforementioned base models, we assemble a comprehensive collection of 28 open-sourced LLMs, ranging in size from 774M (GPT2-Large) to 180B (Falcon-180B). We aimed to gather diverse models covering various parameter sizes. For the widely used LLaMA models, we included LLaMA-7B, 13B, 65B, LLaMA2-7B, and 13B. We also incorporated models with similar architectures to LLaMA, such as InternLM-7B, OpenLLaMA-7B, and Baichuan-7B. To encompass a broader range of parameters, we expanded our collection to include GPT2-Large (Radford et al., 2019), Cerebras-GPT-1.3B (Dey et al., 2023), Qwen-7B, 72B, Galactica-120B, and even the largest Falcon-180B. Additionally, we considered models like MPT-7B, RedPajama-7B (Computer, 2023), ChatGLM-6B (Du et al., 2022), Bloom-7.1B (Workshop et al., 2022), ChatGLM2-6B, Pythia-6.9B

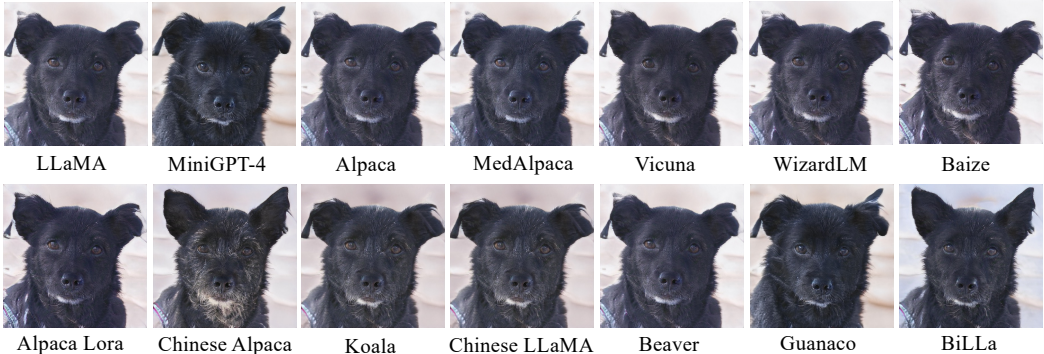


Figure 6: Fingerprints of LLaMA-7B and its offspring models.

and 12B (Biderman et al., 2023), OPT-6.7B and 30B, and GPT-NeoX-20B (Black et al., 2022), among other commonly used LLMs.

We extract invariant terms and calculate ICS between each pair of models. Notably, the similarities between different models were consistently low (Table 5), with an **average ICS of 0.38** (excluding diagonal elements), affirming the effectiveness of invariant terms as quantitative fingerprints.

#### 5.1.4 IDENTIFY 51 OFFSPRING MODELS’ BASE MODEL

To assess the effectiveness of our method, we gathered 51 offspring models derived from 18 distinct base models. (c.f. Appendix A for detailed list and description.) Calculating the ICS between each offspring model and the 18 base models, we predicted the base model with the highest ICS. Comparing these predictions with the ground truth, our method accurately identified the base models for all 51 offspring LLMs, achieving **perfect prediction**.

### 5.2 HUMAN-READABLE FINGERPRINTS FOR QUALITATIVE DISCRIMINATION

In this section, leveraging the invariant terms extracted in the last subsection, we employ the fingerprinting model illustrated in Section 4 to generate human-readable fingerprints for previously mentioned LLMs. Subsequently, we conduct a human subject study to quantitatively assess the human readability of our generated fingerprints.

#### 5.2.1 OFFSPRING MODELS AND CORRESPONDING BASE MODEL’S FINGERPRINTS

We generate fingerprints (Figure 5) for the 7 independently trained LLMs and their offspring models (Section 5.1.1). Notably, for all the offspring models, their fingerprints closely resemble those of their base models. On the other hand, LLMs based on different models yield highly distinctive fingerprints, encompassing various appearances and breeds of dogs.

For LLaMA and its offspring models (Section 5.1.2), their fingerprints align with a similar fingerprint image of a Croatian sheepdog, exhibiting comparable poses, coat patterns, expressions, and backgrounds (Figure 6).

In addition, the fingerprints of the rest offspring models listed in Appendix Table 8 and their respective base models are depicted in Figure 7. Offspring models’ fingerprints still bear high similarity to their base models.

#### 5.2.2 FINGERPRINTS OF 28 INDEPENDENTLY TRAINED LLMs

We also generate fingerprints for the 28 independently trained LLMs (Section 5.1.3), as shown in Figure 8, their fingerprints exhibit high diversity, aligning with the distinct invariant terms of each model.

ICS	GPT2	CGPT	CLM	CLM2	OPT6.7	Py6.9	MPT7	Bat7	Fal7	Inte7	OLM	LM7	Qw7	Bloom	LM27	RedP	Py12	LM213	Bat13	LM13	Neox	LM30	OPT30	Fal40	LM65	Qw72	Gall20	Fall80
GPT2	100.00	18.06	-0.67	0.01	5.50	0.03	0.53	0.16	0.30	0.21	0.05	-0.15	-0.07	-0.45	0.03	-0.04	0.09	0.30	-0.09	0.11	-0.09	3.36	0.79	-0.24	-0.09	-0.37	-1.35	
CGPT	18.06	100.00	-0.29	0.08	7.46	0.14	1.06	0.23	0.48	0.07	0.23	-0.30	0.10	-0.79	-0.18	0.74	0.04	0.01	0.25	0.02	0.05	-0.08	5.10	0.17	0.03	-0.18	-0.18	-1.07
CLM	-0.67	-0.29	100.00	0.18	-1.07	-0.01	-1.32	-0.14	-0.09	-0.18	-0.09	0.15	0.14	0.37	-0.12	0.04	0.10	0.28	-0.03	-0.01	-0.10	-0.07	-0.73	0.17	0.18	0.05	-1.04	0.27
CLM2	0.01	0.08	0.18	100.00	-0.05	0.75	-0.08	0.11	0.87	0.24	0.11	0.11	0.14	-0.79	0.10	0.92	0.69	0.14	0.11	0.09	0.60	-0.02	-0.07	0.30	-0.03	0.07	-0.01	-0.03
OPT6.7	5.50	7.46	-1.07	-0.05	100.00	0.45	5.87	0.41	0.48	-0.06	-0.06	-0.36	-0.14	-1.09	0.02	1.31	0.17	-0.13	0.17	-0.23	0.15	-0.38	46.29	0.65	-0.03	-0.11	-0.17	-1.26
Py6.9	0.03	0.14	-0.01	0.75	0.45	100.00	0.13	0.01	0.66	-0.06	0.04	-0.00	0.01	0.55	0.02	2.37	1.58	0.02	0.01	-0.02	1.41	-0.00	0.29	0.23	-0.01	0.02	-0.01	-0.04
MPT7	0.53	1.06	-1.32	-0.08	5.87	0.13	100.00	0.32	0.44	0.13	0.10	-0.13	0.12	0.83	-0.10	0.62	0.40	-0.18	0.52	-0.03	-0.28	-0.49	1.10	-1.23	-0.33	0.12	-0.61	-0.82
Bat7	0.16	0.23	-0.14	0.11	0.41	0.01	0.32	100.00	0.13	0.21	0.21	0.32	0.41	-0.13	0.35	0.09	0.00	0.22	0.42	0.28	0.04	0.10	0.21	-0.08	0.10	0.31	-0.16	0.01
Fal7	0.30	0.48	-0.09	0.87	0.48	0.66	0.44	0.13	100.00	-0.06	0.04	0.08	0.13	0.48	0.23	0.84	0.62	0.05	0.16	0.01	0.54	0.19	0.39	1.68	0.05	0.19	0.01	-11.07
Inte7	0.21	0.07	-0.18	0.24	-0.06	-0.06	0.13	0.21	-0.06	100.00	0.18	0.03	0.48	-0.01	-0.13	0.02	0.02	0.36	0.13	0.08	-0.00	-0.31	-0.64	0.08	-0.29	-0.26	0.00	-0.01
OLM	0.05	0.23	-0.09	0.11	-0.06	0.04	0.10	0.21	0.04	0.18	100.00	0.32	0.32	0.09	0.39	0.06	0.03	0.23	0.35	0.27	0.05	0.19	0.01	-0.04	0.06	0.32	0.08	-0.06
LM7	-0.15	-0.30	0.15	0.11	-0.36	-0.00	-0.13	0.32	0.08	0.03	0.32	100.00	0.60	0.08	3.16	0.06	0.02	1.64	0.62	2.07	0.00	1.15	0.04	-0.02	1.59	0.67	0.06	0.04
Qw7	-0.07	0.10	0.14	0.14	-0.14	0.01	-0.12	0.41	0.13	0.48	0.32	0.60	100.00	0.01	0.53	-0.02	0.04	0.46	0.57	0.42	-0.00	-0.20	-0.12	-0.08	0.03	0.76	0.11	-0.01
Bloom	-0.45	-0.79	0.37	0.79	-1.09	0.55	0.83	-0.13	0.48	-0.01	0.09	0.08	0.01	100.00	-0.09	0.35	0.48	0.11	0.03	0.07	0.41	0.02	-0.68	0.05	-0.08	0.01	-0.00	-0.18
LM27	-0.04	-0.18	-0.12	0.10	0.02	0.02	-0.10	0.35	0.23	-0.13	0.39	3.16	0.53	-0.09	100.00	-0.04	-0.03	1.45	0.64	1.67	0.02	1.77	0.37	-0.04	1.71	0.87	0.15	0.16
RedP	0.03	0.74	0.04	0.92	1.31	2.37	0.62	0.09	0.84	0.02	0.06	0.06	-0.02	0.35	-0.04	100.00	2.08	-0.00	-0.02	0.03	1.91	-0.13	0.68	0.29	0.03	0.12	0.21	-0.15
Py12	-0.04	0.04	0.10	0.69	0.17	1.58	0.40	0.00	0.62	0.02	0.03	0.02	0.04	0.48	-0.03	2.08	100.00	0.04	-0.01	-0.02	1.27	-0.02	0.08	0.30	-0.04	-0.03	-0.03	-0.00
LM213	0.09	0.01	0.28	0.14	-0.13	0.02	-0.18	0.22	0.05	0.36	0.23	1.64	0.46	0.11	1.45	-0.00	0.04	100.00	0.35	1.03	-0.01	-0.06	-0.39	-0.00	0.15	0.20	-0.06	0.13
Bat13	0.30	0.25	-0.03	0.11	0.17	0.01	0.52	0.42	0.16	0.13	0.35	0.62	0.57	0.03	0.64	-0.02	-0.01	0.35	100.00	0.41	-0.01	0.21	0.21	-0.14	0.25	0.59	0.02	-0.10
LM13	-0.09	0.02	-0.01	0.09	-0.23	-0.02	-0.03	0.28	0.01	0.08	0.27	2.07	0.42	0.07	1.67	0.03	-0.02	1.03	0.41	100.00	-0.01	0.39	0.13	-0.12	0.88	0.37	0.07	-0.04
Neox	0.11	0.05	-0.10	0.60	0.15	1.41	-0.28	0.04	0.54	-0.00	0.05	0.00	-0.00	0.41	0.02	1.91	1.27	-0.01	-0.01	-0.01	100.00	-0.00	0.14	0.34	0.02	0.03	0.11	0.01
LM30	-0.09	-0.08	-0.07	-0.02	-0.38	-0.00	-0.49	0.10	0.19	-0.31	0.19	1.15	-0.20	0.02	1.77	-0.13	-0.02	-0.06	0.21	0.39	-0.00	100.00	0.12	0.08	2.45	0.48	-0.13	0.06
OPT30	3.36	5.10	-0.73	-0.07	46.29	0.29	1.10	0.21	0.39	-0.64	0.01	0.04	-0.12	-0.68	0.37	0.68	0.08	-0.39	0.21	0.13	0.14	0.12	100.00	0.55	0.56	0.40	-0.06	-0.93
Fal40	0.79	0.17	0.17	0.30	0.65	0.23	-1.23	-0.08	1.68	0.08	-0.04	-0.02	-0.08	0.05	-0.04	0.29	0.30	-0.00	-0.14	-0.12	0.34	0.08	0.55	100.00	-0.05	-0.10	0.20	4.90
LM65	-0.24	0.03	0.18	-0.03	-0.03	-0.01	-0.33	0.10	0.05	-0.29	0.06	1.59	0.03	-0.08	1.71	0.03	-0.04	0.15	0.25	0.88	0.02	2.45	0.56	-0.05	100.00	0.44	-0.13	0.02
Qw72	-0.09	-0.18	0.05	0.07	-0.11	0.02	-0.12	0.31	0.19	-0.26	0.32	0.67	0.76	0.01	0.87	0.12	-0.03	0.20	0.59	0.37	0.03	0.48	0.40	-0.10	0.44	100.00	0.07	0.09
Gall20	-0.37	-0.18	-1.04	-0.01	-0.17	-0.01	-0.61	-0.16	0.01	0.00	0.08	0.06	0.11	-0.00	0.15	0.21	-0.03	-0.06	0.02	0.07	0.11	-0.13	-0.06	0.20	-0.13	0.07	100.00	0.19
Fall80	-1.35	-1.07	0.27	-0.03	-1.26	-0.04	-0.82	0.01	-11.07	-0.01	-0.06	0.04	-0.01	-0.18	0.16	-0.15	-0.00	0.13	-0.10	-0.04	0.01	0.06	-0.93	4.90	0.02	0.09	0.19	100.00

Table 5: ICS between 28 open-sourced LLMs (774M to 180B): GPT2-Large (GPT2), Cerebras-GPT-1.3B (CGPT), ChatGLM-6B (CLM), ChatGLM2-6B (CLM2), OPT-6.7B (OPT6.7), Pythia-6.9B (Py6.9), MPT-7B (MPT7), Baichuan-7B (Bat7), Falcon-7B (Fal7), InternLM-7B (OLM), LLaMA-7B (LM7), Qwen-7B (Qw7), LLaMA2-7B (LM27), RedPajamas-7B (RedP), Bloom-7B (Bloom), Pythia-12B (Py12), Baichuan-13B (Bai13), LLaMA-13B (LM13), GPT-NeoX-20B (Neox), LLaMA-30B (LM30), OPT-30B (OPT30), Falcon-40B (Fal40), LLaMA-65B (LM65), Qwen-72B (Qw72), Galactica-120B (Gall20), Falcon-180B (Fall80). Sorted left to right by parameter size from smallest to largest.

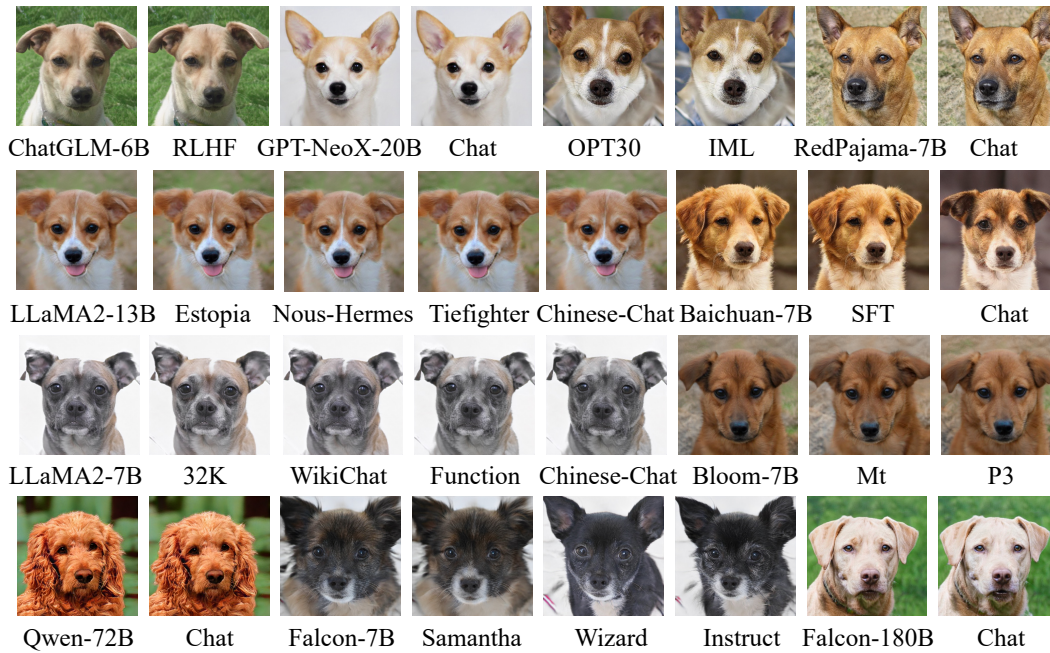


Figure 7: Fingerprints of the other offspring models and their base models.



Figure 8: Fingerprints of 28 independently trained LLMs.

### 5.2.3 HUMAN SUBJECT STUDY

To evaluate the human readability of our generated fingerprints, we generated fingerprints for the 51 offspring LLMs and their 18 base models (Appendix Table 8). We designed a single-choice test with 51 questions, each presenting an offspring model’s fingerprint and asking participants to select

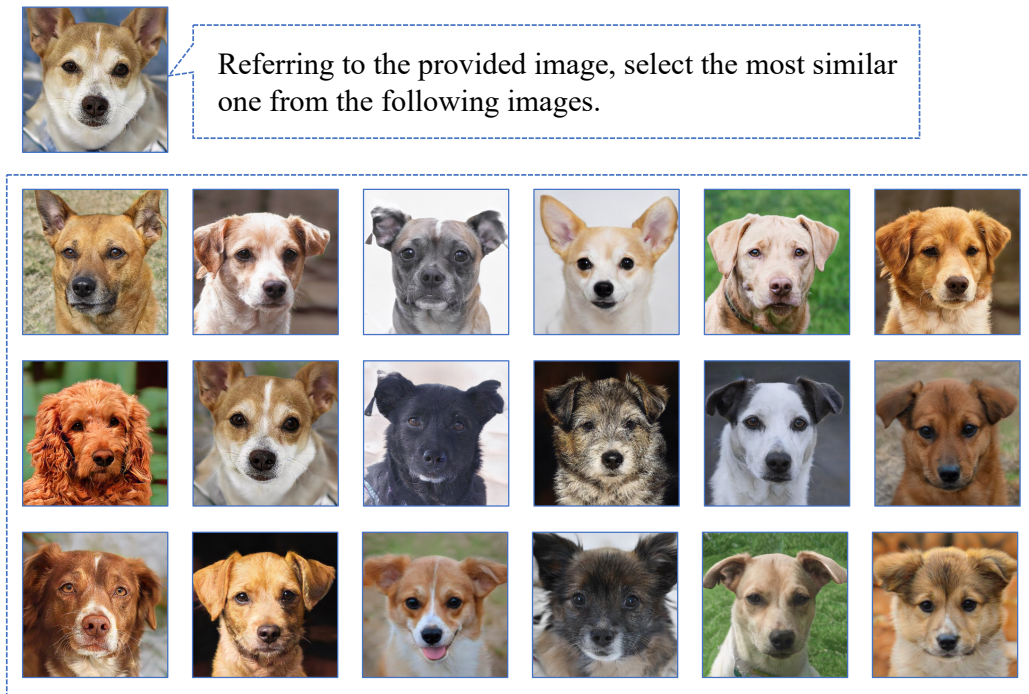


Figure 9: An illustration of a question in the human subject study. Participants were presented with the fingerprint of OPT-IML-30B (finetuned from OPT-30B) and asked to select the most similar image from the fingerprints of 18 distinct base models. Correct responses were counted only when participants precisely selected OPT-30B’s fingerprint.

the most similar image from the fingerprints of the 18 base models (Figure 9). Conducted with 72 college-educated individuals, the test yielded a **94.74% accuracy** rate, highlighting the human readability and intuitive reflection of model similarity in our generated fingerprints.

### 5.3 INDEPENDENTLY TRAINED LLMs IN SMALLER SCALE

To validate the uniqueness and stability of the parameter direction of LLMs trained from scratch, we independently trained GPT-NeoX-350M (Black et al., 2022) models on a subset of the Pile dataset (Gao et al., 2020). First, we examined whether different parameter initializations merely caused by global random seeds result in distinct parameter directions. Second, we explored the variation in the model’s parameter vector direction during pretraining.

#### 5.3.1 GPT-NEOX MODELS WITH DIFFERENT GLOBAL SEEDS

We investigated the impact of global random seeds on the model parameters’ direction by independently training 4 GPT-NeoX-350M models on a subset of the Pile dataset. These models were trained using different global random number seeds while sharing the same architecture, training data batches, computational resources, and hyperparameters.

Subsequently, we computed the cosine similarities between these GPT-NeoX models’ invariant terms, as shown in Table 6. We generated fingerprints for these models, depicted in Figure 10. The results revealed a noteworthy pattern: when GPT-NeoX models are trained from scratch, as long as the global random seed used for parameter initialization is different, it will lead to completely different parameter vector directions after pretraining. Correspondingly, their fingerprints exhibited clear distinctions from each other.

ICS	Seed=1	Seed=2	Seed=3	Seed=4
Seed=1	100.00	2.08	2.23	2.08
Seed=2	2.08	100.00	2.40	2.26
Seed=3	2.23	2.40	100.00	2.29
Seed=4	2.08	2.26	2.29	100.00



Table 6: ICS values between GPT-NeoX models with different global seeds.

Figure 10: Fingerprints of GPT-NeoX models trained with varying global seeds.

Comparing CKPTs	10k-60k	60k-110k	110k-160k	160k-210k	210k-260k	260k-310k	310k-360k
Cosine similarity	56.23	84.65	88.95	90.96	92.13	93.22	94.25

Table 7: Cosine similarities between neighboring checkpoints (saved every 50k steps) of GPT-NeoX models during pretraining.

### 5.3.2 MODEL’S PARAMETER VECTOR DIRECTION’S VARIATIONS DURING PRETRAINING

In addition, we have explored the variation in the model’s parameter vector direction during pre-training by comparing neighboring checkpoints of a model and calculating their cosine similarities. Specifically, we trained a GPT-NeoX-350M model on a subset of the Pile dataset for 360,000 steps and saved a checkpoint every 50k steps. As pretraining progresses, we observed a diminishing change in the model’s parameter direction, leading to gradual stabilization, as shown in Table 7. For larger models and more pretraining steps, we expect this phenomenon to be more pronounced, indicating that the parameter direction of LLMs tends to stabilize during pretraining.

## 6 CONCLUSION

In this paper, we introduce a novel approach that uses model parameters to yield a fingerprint for LLMs. Our approach offers a dual benefit by providing a human-readable identity for qualitative discrimination and invariant terms for quantitative verification of LLMs. Different from the well-studied black-box or white-box settings, our method lies in the middle of both. Although generating the invariant terms needs access to the model parameters, which has to be done by the LLM owners and might need regulations to prevent fake terms, all the subsequent steps could be done by the public, without requiring a special third-party institution. Moreover, as only the invariant terms and fingerprint images are published, no model weights need to be exposed outside of its owner, neither to the public nor the other LLM owners, during the whole process.

## REFERENCES

Yossi Adi, Carsten Baum, Moustapha Cisse, Benny Pinkas, and Joseph Keshet. Turning your weakness into a strength: Watermarking deep neural networks by backdooring. In *27th USENIX Security Symposium (USENIX Security 18)*, pp. 1615–1631, 2018.

Ebtesam Almazrouei, Hamza Alobeidli, Abdulaziz Alshamsi, Alessandro Cappelli, Ruxandra Cojocaru, Mérouane Debbah, Étienne Goffinet, Daniel Hesslow, Julien Launay, Quentin Malartic, et al. The falcon series of open language models. *arXiv preprint arXiv:2311.16867*, 2023.

Jinze Bai, Shuai Bai, Yunfei Chu, Zeyu Cui, Kai Dang, et al. Qwen technical report. *arXiv preprint arXiv:2309.16609*, 2023.

Yuntao Bai, Andy Jones, Kamal Ndousse, Amanda Askell, Anna Chen, Nova DasSarma, Dawn Drain, Stanislav Fort, Deep Ganguli, Tom Henighan, et al. Training a helpful and harmless assistant with reinforcement learning from human feedback. *arXiv preprint arXiv:2204.05862*, 2022.

BaiChuan-Inc. <https://github.com/baichuan-inc/Baichuan-7B>, 2023.

- Stella Biderman, Hailey Schoelkopf, Quentin Gregory Anthony, Herbie Bradley, Kyle O’Brien, Eric Hallahan, Mohammad Aflah Khan, Shivanshu Purohit, USVSN Sai Prashanth, Edward Raff, et al. Pythia: A suite for analyzing large language models across training and scaling. In *International Conference on Machine Learning*, pp. 2397–2430. PMLR, 2023.
- Yonatan Bisk, Rowan Zellers, Jianfeng Gao, Yejin Choi, et al. Piqa: Reasoning about physical commonsense in natural language. In *Proceedings of the AAAI conference on artificial intelligence*, pp. 7432–7439, 2020.
- Sidney Black, Stella Biderman, Eric Hallahan, Quentin Anthony, Leo Gao, Laurence Golding, Horace He, Connor Leahy, Kyle McDonell, Jason Phang, et al. Gpt-neox-20b: An open-source autoregressive language model. In *Proceedings of BigScience Episode# 5–Workshop on Challenges & Perspectives in Creating Large Language Models*, pp. 95–136, 2022.
- Franziska Boenisch. A systematic review on model watermarking for neural networks. *Frontiers in big Data*, 4:729663, 2021.
- Tom Brown, Benjamin Mann, Nick Ryder, Melanie Subbiah, Jared D Kaplan, Prafulla Dhariwal, Arvind Neelakantan, Pranav Shyam, Girish Sastry, Amanda Askell, et al. Language models are few-shot learners. *Advances in neural information processing systems*, 33:1877–1901, 2020.
- Yunjey Choi, Youngjung Uh, Jaejun Yoo, and Jung-Woo Ha. Stargan v2: Diverse image synthesis for multiple domains. In *Proceedings of the IEEE/CVF conference on computer vision and pattern recognition*, pp. 8188–8197, 2020.
- Aakanksha Chowdhery, Sharan Narang, Jacob Devlin, Maarten Bosma, Gaurav Mishra, Adam Roberts, Paul Barham, Hyung Won Chung, Charles Sutton, Sebastian Gehrmann, et al. Palm: Scaling language modeling with pathways. *arXiv preprint arXiv:2204.02311*, 2022.
- Miranda Christ, Sam Gunn, and Or Zamir. Undetectable watermarks for language models. *arXiv preprint arXiv:2306.09194*, 2023.
- Christopher Clark, Kenton Lee, Ming-Wei Chang, Tom Kwiatkowski, Michael Collins, and Kristina Toutanova. Boolq: Exploring the surprising difficulty of natural yes/no questions. *arXiv preprint arXiv:1905.10044*, 2019.
- Peter Clark, Isaac Cowhey, Oren Etzioni, Tushar Khot, Ashish Sabharwal, Carissa Schoenick, and Oyvind Tafjord. Think you have solved question answering? try arc, the ai2 reasoning challenge. *arXiv preprint arXiv:1803.05457*, 2018.
- Together Computer. Redpajama: An open source recipe to reproduce llama training dataset, 2023. URL <https://github.com/togethercomputer/RedPajama-Data>.
- Mike Conover, Matt Hayes, Ankit Mathur, Jianwei Xie, Jun Wan, Sam Shah, Ali Ghodsi, Patrick Wendell, Matei Zaharia, and Reynold Xin. Free dolly: Introducing the world’s first truly open instruction-tuned llm, 2023.
- Yiming Cui, Ziqing Yang, and Xin Yao. Efficient and effective text encoding for chinese llama and alpaca. *arXiv preprint arXiv:2304.08177*, 2023.
- Tim Dettmers, Artidoro Pagnoni, Ari Holtzman, and Luke Zettlemoyer. Qlora: Efficient finetuning of quantized llms. *arXiv preprint arXiv:2305.14314*, 2023.
- Nolan Dey, Gurpreet Gosal, Hemant Khachane, William Marshall, Ribhu Pathria, Marvin Tom, Joel Hestness, et al. Cerebras-gpt: Open compute-optimal language models trained on the cerebras wafer-scale cluster. *arXiv preprint arXiv:2304.03208*, 2023.
- Zhengxiao Du, Yujie Qian, Xiao Liu, Ming Ding, Jiezhong Qiu, Zhilin Yang, and Jie Tang. Glm: General language model pretraining with autoregressive blank infilling. In *Proceedings of the 60th Annual Meeting of the Association for Computational Linguistics (Volume 1: Long Papers)*, pp. 320–335, 2022.

- Leo Gao, Stella Biderman, Sid Black, Laurence Golding, Travis Hoppe, Charles Foster, Jason Phang, Horace He, Anish Thite, Noa Nabeshima, et al. The pile: An 800gb dataset of diverse text for language modeling. *arXiv preprint arXiv:2101.00027*, 2020.
- Xinyang Geng. EasyLM: A simple and scalable training framework for large language models, 2023. URL <https://github.com/young-geng/EasyLM>.
- Xinyang Geng and Hao Liu. Openllama: An open reproduction of llama, May 2023. URL [https://github.com/openlm-research/open\\_llama](https://github.com/openlm-research/open_llama).
- OpenAI GPT-4. Gpt-4 technical report. *ArXiv*, abs/2303.08774, 2023.
- Chenxi Gu, Chengsong Huang, Xiaoqing Zheng, Kai-Wei Chang, and Cho-Jui Hsieh. Watermarking pre-trained language models with backdooring. *arXiv preprint arXiv:2210.07543*, 2022.
- Tianyu Han, Lisa C Adams, Jens-Michalis Papaioannou, Paul Grundmann, Tom Oberhauser, Alexander Löser, Daniel Truhn, and Keno K Bresssem. Medalpaca—an open-source collection of medical conversational ai models and training data. *arXiv preprint arXiv:2304.08247*, 2023.
- Dan Hendrycks, Collin Burns, Steven Basart, Andy Zou, Mantas Mazeika, Dawn Song, and Jacob Steinhardt. Measuring massive multitask language understanding. In *International Conference on Learning Representations*, 2020.
- Jordan Hoffmann, Sebastian Borgeaud, Arthur Mensch, Elena Buchatskaya, Trevor Cai, Eliza Rutherford, Diego de Las Casas, Lisa Anne Hendricks, Johannes Welbl, Aidan Clark, et al. Training compute-optimal large language models. *arXiv preprint arXiv:2203.15556*, 2022.
- Tero Karras, Samuli Laine, and Timo Aila. A style-based generator architecture for generative adversarial networks. In *Proceedings of the IEEE/CVF conference on computer vision and pattern recognition*, pp. 4401–4410, 2019.
- Tero Karras, Samuli Laine, Miika Aittala, Janne Hellsten, Jaakko Lehtinen, and Timo Aila. Analyzing and improving the image quality of stylegan. In *Proceedings of the IEEE/CVF conference on computer vision and pattern recognition*, pp. 8110–8119, 2020.
- John Kirchenbauer, Jonas Geiping, Yuxin Wen, Jonathan Katz, Ian Miers, and Tom Goldstein. A watermark for large language models. In Andreas Krause, Emma Brunskill, Kyunghyun Cho, Barbara Engelhardt, Sivan Sabato, and Jonathan Scarlett (eds.), *Proceedings of the 40th International Conference on Machine Learning*, volume 202 of *Proceedings of Machine Learning Research*, pp. 17061–17084. PMLR, 23–29 Jul 2023. URL <https://proceedings.mlr.press/v202/kirchenbauer23a.html>.
- Andreas Köpf, Yannic Kilcher, Dimitri von Rütte, Sotiris Anagnostidis, Zhi-Rui Tam, Keith Stevens, Abdullah Barhoum, Nguyen Minh Duc, Oliver Stanley, Richárd Nagyfi, et al. Openassistant conversations—democratizing large language model alignment. *arXiv preprint arXiv:2304.07327*, 2023.
- Kalpesh Krishna, Yixiao Song, Marzena Karpinska, John Wieting, and Mohit Iyyer. Paraphrasing evades detectors of ai-generated text, but retrieval is an effective defense. *arXiv preprint arXiv:2303.13408*, 2023.
- Guokun Lai, Qizhe Xie, Hanxiao Liu, Yiming Yang, and Eduard Hovy. Race: Large-scale reading comprehension dataset from examinations. In *Proceedings of the 2017 Conference on Empirical Methods in Natural Language Processing*, pp. 785–794, 2017.
- Linyang Li, Pengyu Wang, Ke Ren, Tianxiang Sun, and Xipeng Qiu. Origin tracing and detecting of llms. *arXiv preprint arXiv:2304.14072*, 2023.
- Zhongli Li. Billa: A bilingual llama with enhanced reasoning ability. <https://github.com/Neutralzz/BiLLa>, 2023.
- Kevin Lin, Chung-Ching Lin, Lin Liang, Zicheng Liu, and Lijuan Wang. Mpt: Mesh pre-training with transformers for human pose and mesh reconstruction. *arXiv preprint arXiv:2211.13357*, 2022.



- Eric Mitchell, Yoonho Lee, Alexander Khazatsky, Christopher D. Manning, and Chelsea Finn. Detectgpt: Zero-shot machine-generated text detection using probability curvature. In Andreas Krause, Emma Brunskill, Kyunghyun Cho, Barbara Engelhardt, Sivan Sabato, and Jonathan Scarlett (eds.), *International Conference on Machine Learning, ICML 2023, 23-29 July 2023, Honolulu, Hawaii, USA*, volume 202 of *Proceedings of Machine Learning Research*, pp. 24950–24962. PMLR, 2023. URL <https://proceedings.mlr.press/v202/mitchell23a.html>.
- OpenAI. Introducing chatgpt. 2022. URL <https://openai.com/blog/chatgpt>.
- OpenAI. Ai classifier. 2023. URL <https://beta.openai.com/ai-text-classifier>.
- Guilherme Penedo, Quentin Malartic, Daniel Hesslow, Ruxandra Cojocaru, Alessandro Cappelli, Hamza Alobeidli, Baptiste Pannier, Ebtesam Almazrouei, and Julien Launay. The RefinedWeb dataset for Falcon LLM: outperforming curated corpora with web data, and web data only. *arXiv preprint arXiv:2306.01116*, 2023. URL <https://arxiv.org/abs/2306.01116>.
- Alec Radford, Jeffrey Wu, Rewon Child, David Luan, Dario Amodei, Ilya Sutskever, et al. Language models are unsupervised multitask learners. *OpenAI blog*, 1(8):9, 2019.
- Vinu Sankar Sadasivan, Aounon Kumar, Sriram Balasubramanian, Wenxiao Wang, and Soheil Feizi. Can ai-generated text be reliably detected? *arXiv preprint arXiv:2303.11156*, 2023.
- Keisuke Sakaguchi, Ronan Le Bras, Chandra Bhagavatula, and Yejin Choi. Winogrande: An adversarial winograd schema challenge at scale. *Communications of the ACM*, 64(9):99–106, 2021.
- Rohan Taori, Ishaan Gulrajani, Tianyi Zhang, Yann Dubois, Xuechen Li, Carlos Guestrin, Percy Liang, and Tatsunori B. Hashimoto. Stanford alpaca: An instruction-following llama model. [https://github.com/tatsu-lab/stanford\\_alpaca](https://github.com/tatsu-lab/stanford_alpaca), 2023.
- Ross Taylor, Marcin Kardas, Guillem Cucurull, Thomas Scialom, Anthony Hartshorn, Elvis Saravia, Andrew Poulton, Viktor Kerkez, and Robert Stojnic. Galactica: A large language model for science. *arXiv preprint arXiv:2211.09085*, 2022.
- InternLM Team. Internlm: A multilingual language model with progressively enhanced capabilities. <https://github.com/InternLM/InternLM>, 2023.
- Edward Tian. Gptzero: An ai text detector. 2023. URL <https://gptzero.me/>.
- Hugo Touvron, Thibaut Lavril, Gautier Izacard, Xavier Martinet, Marie-Anne Lachaux, Timothée Lacroix, Baptiste Rozière, Naman Goyal, Eric Hambro, Faisal Azhar, et al. Llama: Open and efficient foundation language models. *arXiv preprint arXiv:2302.13971*, 2023a.
- Hugo Touvron, Louis Martin, Kevin Stone, Peter Albert, Amjad Almahairi, Yasmine Babaei, Nikolay Bashlykov, Soumya Batra, Prajjwal Bhargava, Shrutli Bhosale, et al. Llama 2: Open foundation and fine-tuned chat models. *arXiv preprint arXiv:2307.09288*, 2023b.
- Yusuke Uchida, Yuki Nagai, Shigeyuki Sakazawa, and Shin’ichi Satoh. Embedding watermarks into deep neural networks. In *Proceedings of the 2017 ACM on International Conference on Multimedia Retrieval*. ACM, jun 2017. doi: 10.1145/3078971.3078974. URL <https://doi.org/10.1145%2F3078971.3078974>.
- Eric J. Wang. <https://github.com/tloen/alpaca-lora>, 2023.
- Jiangfeng Wang, Hanzhou Wu, Xinpeng Zhang, and Yuwei Yao. Watermarking in deep neural networks via error back-propagation. *Electronic Imaging*, 2020(4):22–1, 2020.
- Tianhao Wang and Florian Kerschbaum. Attacks on digital watermarks for deep neural networks. In *ICASSP 2019-2019 IEEE International Conference on Acoustics, Speech and Signal Processing (ICASSP)*, pp. 2622–2626. IEEE, 2019.
- BigScience Workshop, Teven Le Scao, Angela Fan, Christopher Akiki, Ellie Pavlick, Suzana Ilić, Daniel Hesslow, Roman Castagné, Alexandra Sasha Luccioni, François Yvon, et al. Bloom: A 176b-parameter open-access multilingual language model. *arXiv preprint arXiv:2211.05100*, 2022.

- Kangxi Wu, Liang Pang, Huawei Shen, Xueqi Cheng, and Tat-Seng Chua. Llm-det: A large language models detection tool. *arXiv preprint arXiv:2305.15004*, 2023a.
- Shijie Wu, Ozan Irsoy, Steven Lu, Vadim Dabravolski, Mark Dredze, Sebastian Gehrmann, Prabhajan Kambadur, David Rosenberg, and Gideon Mann. Bloomberggpt: A large language model for finance. *arXiv preprint arXiv:2303.17564*, 2023b.
- Tao Xiang, Chunlong Xie, Shangwei Guo, Jiwei Li, and Tianwei Zhang. Protecting your nlg models with semantic and robust watermarks. *arXiv preprint arXiv:2112.05428*, 2021.
- Can Xu, Qingfeng Sun, Kai Zheng, Xiubo Geng, Pu Zhao, Jiazhan Feng, Chongyang Tao, and Daxin Jiang. Wizardlm: Empowering large language models to follow complex instructions. *arXiv preprint arXiv:2304.12244*, 2023a.
- Canwen Xu, Daya Guo, Nan Duan, and Julian McAuley. Baize: An open-source chat model with parameter-efficient tuning on self-chat data. *arXiv preprint arXiv:2304.01196*, 2023b.
- Mohammad Mehdi Yadollahi, Farzaneh Shoeleh, Sajjad Dadkhah, and Ali A Ghorbani. Robust black-box watermarking for deep neural network using inverse document frequency. In *2021 IEEE Intl Conf on Dependable, Autonomic and Secure Computing, Intl Conf on Pervasive Intelligence and Computing, Intl Conf on Cloud and Big Data Computing, Intl Conf on Cyber Science and Technology Congress (DASC/PiCom/CBDCom/CyberSciTech)*, pp. 574–581. IEEE, 2021.
- Rowan Zellers, Ari Holtzman, Yonatan Bisk, Ali Farhadi, and Yejin Choi. Hellaswag: Can a machine really finish your sentence? In *Proceedings of the 57th Annual Meeting of the Association for Computational Linguistics*, pp. 4791–4800, 2019.
- Richard Zhang, Phillip Isola, Alexei A Efros, Eli Shechtman, and Oliver Wang. The unreasonable effectiveness of deep features as a perceptual metric. In *Proceedings of the IEEE conference on computer vision and pattern recognition*, pp. 586–595, 2018.
- Susan Zhang, Stephen Roller, Naman Goyal, Mikel Artetxe, Moya Chen, Shuohui Chen, Christopher Dewan, Mona Diab, Xian Li, Xi Victoria Lin, et al. Opt: Open pre-trained transformer language models. *arXiv preprint arXiv:2205.01068*, 2022.
- Lianmin Zheng, Wei-Lin Chiang, Ying Sheng, Siyuan Zhuang, Zhanghao Wu, Yonghao Zhuang, Zi Lin, Zhuohan Li, Dacheng Li, Eric Xing, et al. Judging llm-as-a-judge with mt-bench and chatbot arena. *arXiv preprint arXiv:2306.05685*, 2023a.
- Qinkai Zheng, Xiao Xia, Xu Zou, Yuxiao Dong, Shan Wang, Yufei Xue, Zihan Wang, Lei Shen, Andi Wang, Yang Li, Teng Su, Zhilin Yang, and Jie Tang. Codegeex: A pre-trained model for code generation with multilingual evaluations on humaneval-x. In *KDD*, 2023b.
- Deyao Zhu, Jun Chen, Xiaoqian Shen, Xiang Li, and Mohamed Elhoseiny. Minigpt-4: Enhancing vision-language understanding with advanced large language models. *arXiv preprint arXiv:2304.10592*, 2023.

Offspring Model	Base Model	Detail
Alpaca	LLaMA-7B	SFT on Stanford’s instruction-following data
Alpaca-Lora	LLaMA-7B	SFT used the Lora training method
MiniGPT-4	LLaMA-7B	multimodal model aligned on 5 million image-text pairs
Chinese-LLaMA	LLaMA-7B	continued pretraining on Chinese corpus
Chinese-Alpaca	LLaMA-7B	continued pretraining and finetuned on Chinese corpus
Vicuna	LLaMA-7B	SFT on around 125K user-shared conversations
Baize	LLaMA-7B	finetuned on 100k ChatGPT generated dialogs
Koala	LLaMA-7B	SFT on dialogue data gathered from the web
WizardLM	LLaMA-7B	trained on complex instructions data
MedAlpaca	LLaMA-7B	finetuned on medical datasets
Beaver	LLaMA-7B	underwent RLHF
Guanaco	LLaMA-7B	finetuned on nearly 600K multilingual dataset
BiLLa	LLaMA-7B	continued pretraining on a new language
Falcon-40B-Instruct	Falcon-40B	finetuned on a mixture of Baize
Falcon-40B-SFT-Top1-560	Falcon-40B	SFT based on the OASST dataset (Köpf et al., 2023)
MPT-7B-Instruct	MPT-7B	finetuned on Dolly2 and HH-RLHF (Bai et al., 2022)
MPT-7B-StoryWriter	MPT-7B	finetuned with super long context length
MPT-7B-Chat	MPT-7B	finetuned on a mixture of instruct datasets
Qwen-7B-Chat	Qwen-7B	trained with alignment techniques
Firefly-Qwen-7B	Qwen-7B	SFT by the Firefly project
Baichuan-13B-Chat	Baichuan-13B	dialogue version
Baichuan-13B-SFT	Baichuan-13B	bilingual instruction-tuned model
InternLM-7B-Chat	InternLM-7B	optimized for dialogue use cases
Firefly-InternLM	InternLM-7B	SFT by the Firefly project
Qwen-72B-Chat	Qwen-72B	trained with alignment techniques
OPT-IML-30B	OPT-30B	trained on 1500 tasks gathered from 8 NLP benchmarks
ChatGLM-fitness-RLHF	ChatGLM-6B	RLHF and SFT on millions data
GPT-NeoXT-Chat	GPT-NeoX-20B	fine-tuned with 43 million high-quality instructions
RedPajama-Chat	RedPajama-7B	fine-tuned on OASST1 and Dolly2 (Conover et al., 2023)
Bloomz-p3	Bloom-7B	finetuned on crosslingual task(P3)
Bloomz-mt	Bloom-7B	multitask finetuned on xP3mt
Falcon-180B-Chat	Falcon-180B	finetuned on a mixture of instruct datasets
LLaMA2-7B-Chat	LLaMA2-7B	dialogue version
LLaMA2-7B-32K	LLaMA2-7B	continued pretraining and SFT to enhance long-context capacity
LLaMA2-function-calling	LLaMA2-7B	extends LLaMA2 model with function calling capabilities
Llama2-Chinese-7B	LLaMA2-7B	aligned with Chinese dataset
Vicuna2	LLaMA2-7B	fine-tuned on user-shared conversations
LLaMA2-WikiChat	LLaMA2-7B	fine-tuned LLaMA-2 to retrieve data from Wikipedia
Falcon-7B-Instruct	Falcon-7B	finetuned on a 250M tokens mixture of instruct/chat datasets
Samantha-Falcon-7B	Falcon-7B	finetuned in philosophy, psychology, and personal relationships
WizardLM-Falcon-7B	Falcon-7B	WizardLM trained on top of Falcon-7B
MPT-30B-Chat	MPT-30B	finetuned on a mixture of instruct datasets
MPT-30B-Instruct	MPT-30B	finetuned on Dolly2 and HH-RLHF
Baichuan-7B-SFT	Baichuan-7B	bilingual instruction-tuned model
Baichuan-7B-Chat	Baichuan-7B	dialogue version
LLaMA2-13B-Chat	LLaMA2-13B	optimized for dialogue use cases
LLaMA2-French	LLaMA2-13B	fine-tuned for answer questions in French
LLaMA2-Estopia	LLaMA2-13B	focused on improving the dialogue and prose
LLaMA2-Tiefighter	LLaMA2-13B	merging two different Lora’s
Llama2-Chinese-13B	LLaMA2-13B	aligned with Chinese dataset
Nous-Hermes-Llama2-13B	LLaMA2-13B	fine-tuned on over 300,000 instructions

Table 8: Detailed descriptions of all 51 offspring models.

## APPENDICES

## A 51 OFFSPRING MODELS

Please see Table 8 for detailed list and description of all offspring models.

## B IMPLEMENTATION DETAILS OF THE FINGERPRINTING MODEL

### B.1 TRAINING SETTINGS

In the training stage, we alternate training the discriminator and CNN encoder every 10 steps. We set the batch size to 10, the initial learning rate to 0.0001, and introduce a noise intensity  $\alpha$  of 0.16 for positive samples. After 16 epochs of training, we obtained the CNN encoder used in our paper.

### B.2 MODEL ARCHITECTURE

For the CNN encoder: The CNN encoder takes invariant terms  $M \in \mathbb{R}^{4096 \times 4096 \times 6}$  as input and produces a feature vector  $v$  as output. Our CNN encoder structure, as depicted in Figure 4, consists of the first four convolutional layers and the last mean pooling layer. The mean pooling layer simply calculates the average of the feature maps obtained from each channel, resulting in a feature vector  $v$  with a length equal to the number of channels. The hyperparameters for the four convolutional layers are provided in the table below:

CNN Layers	Input Channel	Output Channel	Kernel Size	Stride	Padding
Layer 1	6	8	48	4	22
Layer 2	8	64	48	4	22
Layer 3	64	256	48	4	22
Layer 4	256	512	48	4	22

Table 9: Detailed hyperparameters of the stacked four convolutional layers.

For the discriminator: We utilize a simple 3-layer MLP as the discriminator. The 512-dimensional feature vector  $v$  from the CNN encoder serves as fake data, while a 512-dimensional vector  $x$  sampled from the standard normal distribution serves as real data. The discriminator processes  $v$  and  $x$ , progressively reducing dimensionality through three linear layers, and finally outputs the probability of a sample being real after applying a sigmoid activation function. The sizes of the three linear layers are  $W_1 \in \mathbb{R}^{512 \times 256}$ ,  $W_2 \in \mathbb{R}^{256 \times 128}$ , and  $W_3 \in \mathbb{R}^{128 \times 128}$ , respectively.

For the image generator: The pretrained StyleGAN2 checkpoint we used can be found at:

<https://nvlabs-fi-cdn.nvidia.com/stylegan2-ada-pytorch/pretrained/afhqdqg.pkl>